Estimating Directed Connectivity with OPM-MEG: A Feasibility Study

Mangor Pedersen[1*], Geet Vashista[1], Dion Henare[1] and Paul F. Sowman[2,3]

1. Department of Psychology and Neuroscience, Auckland University of Technology, Auckland, New Zealand
2. Department of Physiotherapy, School of Clinical Sciences, Auckland University of Technology, Auckland, New Zealand
3. Faculty of Medicine, Health and Human Sciences, Macquarie University, Sydney, Australia

[*]Correspondence to: Mangor Pedersen. Auckland University of Technology (AUT), Auckland, New Zealand. E-mail address: mangor.pedersen@aut.ac.nz

Keywords: OPM-MEG, magnetoencephalography, directed connectivity, transfer entropy

Abstract

We investigated the feasibility of using directed connectivity analysis for magnetoencephalography data recorded via Optically Pumped Magnetometers (OPM-MEG). Ten healthy adult participants were scanned twice in an OPM-MEG system, and Beamformer source localisation was employed to obtain source time series within 62 cortical brain regions. Multivariate transfer entropy (mTE) was used to quantify directed connectivity, with lags ranging from 1 to 10 time points. Our findings showed that out-degree connectivity (node to network) in somatomotor and attention networks was higher than in other networks. In contrast, in-degree connectivity (network to node) was not different between networks. Longer time lags were associated with shorter physical distances between nodes. Transfer entropy networks demonstrated a small-world network topology, reinforcing the biological plausibility of our findings. Brain connections with higher transfer entropy values exhibited a stronger Phase Lag Index and Pearson's correlation coefficient than non-significant transfer entropy connections, suggesting a relationship between directed and non-directed connectivity measures. All results were consistent across the two scans. OPM-MEG research is likely to expand significantly, and based on our preliminary findings, we propose that directed connectivity measures may provide valuable insights into the underlying mechanisms of brain communication.

Background

Rapid advances in quantum physics are changing the field of neuroscience. A prime example is the recent advent of the OPM-MEG scanner (Boto et al., 2018). OPM-MEG records fast neural activity at the millisecond scale, overcoming common temporal limitations of techniques such as fMRI (Boto et al., 2019; Hill et al., 2020, 2022; Jas et al., 2021; Mellor et al., 2021; Roberts et al., 2019) and it is not susceptible to volume conduction, overcoming source localization and functional connectivity limitations of EEG (Brookes et al., 2022). OPM-MEG works by measuring magnetic fields generated by current flow in assemblies of neurons in the brain, enabled by recording OPM-MEG in a shielded room that deflects any interference from the earth's magnetic field (Holmes et al., 2022; Iivanainen et al., 2019; Seymour et al., 2022). In a room with virtually no magnetic field from the earth, OPMs use light/laser to cause a state transition in magnetically susceptible Alkali vapours, enabling detection of the magnetic field from ensembles of neurons when they activate in the brain (Tierney et al., 2019). While Alkali-based sensors are used in this study, it is worth noting that helium-4 OPM sensors are also emerging (Fourcault et al., 2021). An advantage of OPM-MEG is that its magnetic field recording ability is less affected by confounds and artefacts commonly associated with traditional neuroscience equipment, such as head motion, allowing users to be mobile during a scan. Such advances open up research possibilities in challenging cohorts such as children and clinical populations, including people with seizures and movement disorders (Feys et al., 2022; Mellor et al., 2021; Pedersen et al., 2022; Vivekananda et al., 2020).

Pioneering OPM-MEG research has emerged in recent years, which suggests that the performance of OPM-MEG is comparable to that of SQUID-based MEG systems (Boto et al., 2019). Recent reports have demonstrated the capability of correlation-based connectivity methods to derive functional connectivity patterns from the OPM-MEG data (Boto et al., 2021) with good test-retest reliability (Rier et al., 2023). However, the field still needs evidence of whether directed connectivity is feasible with OPM-MEG. The most common directed connectivity measures include the model-based Dynamic Causal Modelling Field (Friston et al., 2003), as well as the Granger Causality Field (Granger, 1969) and Transfer Entropy (Schreiber, 2000). We used Transfer Entropy in this study due to its advantageous multivariate and non-parametric properties (Novelli et al., 2019). The primary objective of our research study was to investigate various aspects of directed connectivity utilising OPM-MEG combined with Multivariate Transfer Entropy (mTE - Novelli et al., 2019; Wollstadt et al., 2019). This statistical measure based on information theory quantifies the information transferred from one time series to another, encompassing the input and output of the information flow (Schreiber, 2000). Unlike other measures, mTE connectivity matrices are asymmetric, allowing us to quantify the information going *to and from* different regions with a

specific temporal distance – i.e., at one particular temporal lag. Consequently, mTE provides a framework for investigating the directed flow of information between various brain regions, shedding light on the specific communication pathways within the brain.

The main objective of this study was to investigate the performance of mTE-based directed connectivity measures using OPM-MEG data, extending previous work from non-directed connectivity findings in OPM-MEG (Boto et al., 2021; Rier et al., 2023) as well as other methodologies (Betzel et al., 2013; Bullmore & Sporns, 2009; Sporns, 2013; van den Heuvel et al., 2008). Our study had several specific aims to assess the performance of OPM-MEG mTE. Firstly, we wanted to determine if OPM-MEG mTE shows different lag structures across various resting-state networks. We hypothesised that mTE lags would vary between networks, reflecting the different information processing rates observed in distinct neuronal circuitries (Young et al., 2019). Secondly, we aimed to explore whether OPM-MEG mTE exhibits small-world network topology, a common feature of all brain networks (Watts & Strogatz, 1998), providing biological plausibility for mTE lag-based networks. Next, we examined the relationship between Transfer Entropy and the physical distance between OPM-MEG-derived brain sources to assess whether mTE captures the association between physical brain properties and mTE. We further investigated the correlation between mTE and other commonly used connectivity measures, such as the Phase Lag Index and Pearson's correlation coefficient, to determine if mTE is related to other connectivity measures. Lastly, we tested for any hemispheric differences between mTE nodes and consistency in mTE findings across two scans to estimate the reliability of the OPM-MEG-based mTE. By investigating these objectives, our study provides valuable insights into the capabilities and characteristics of OPM-MEG-based mTE in estimating directed connectivity.

Results

For each of the ten subjects (each scanned twice) who watched a 600-second video, we downsampled the OPM-MEG data at a factor of 10, from 1200Hz to 120Hz, before band-pass filtering the data between 1 and 48 Hz. We then used a Beamformer analysis to obtain time-series from 62 cortical sources based on the AAL parcellation atlas (Tzourio-Mazoyer et al., 2002). These parcel-derived time series constitute the nodes in our network analysis. Next, we used multivariate transfer entropy (mTE) using the IDTxl toolbox to measure directed connectivity (Wollstadt et al., 2019). In the multivariate case of transfer entropy, mTE estimates how much information from the past of one variable helps forecast the future values of another variable while considering the influence of other variables in the system (Novelli et al., 2019 – see also the methods section for more information). For each subject, the output of mTE is an asymmetric directed connectivity

matrix with a size of 62x62 nodes. Values in these matrices are the optimal lag between significant connections rather than connection strength (most common in other studies), and their values range between 1 and 10 time points. We calculated their node degree after generating directed connectivity matrices (Rubinov & Sporns, 2010). The node degree represents the sum of connections for each node. Due to the asymmetric nature of these matrices, we quantified the directed information flow to and from nodes, denoted In- and Out-Degree, respectively. As seen in Figure 1 (left), the red node influences other network nodes, i.e., it has a high Out-Degree. Conversely, in the node in Figure 1 (right), other nodes influence the target nodes. In our study, a stronger degree value indicates longer lags of nodes by summarising lags from incoming nodes (In-Degree) and outgoing nodes (Out-Degree).

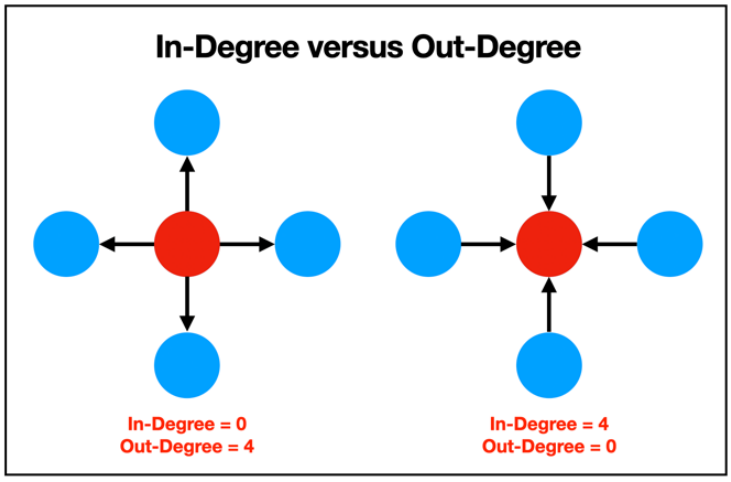

Figure 1: Two toy networks describing the difference between In- and Out-Degree. Left network: a network with low In-Degree and high Out-Degree. Right: a network with high In-Degree and low Out-Degree.

Network-specific mTE effects for Out-Degree but not In-Degree:

In our first analysis, we explored In- and Out-Degree for significant mTE connections in six resting-state networks (Yeo et al., 2011), including the visual network (VIS), somatomotor network (SMN), attention network (ATT), frontoparietal network (FPN) and default mode network (DMN). For the limbic system (LIMBIC), only nodes from the orbitofrontal cortex were selected as we did not study deep brain regions in this study. For Out-Degree, we observed a significant difference between networks in session 1: $F(5,54) = 8.25$, $p < 0.001$. SMN had a greater Out-Degree than VIS ($p = 0.004$), LIMBIC ($p < 0.001$) and DMN ($p = 0.007$), and LIMBIC had a shorter mean lag than ATT ($p < 0.001$) and FPN ($p = 0.003$). In session 2, a similar trend was seen: $F(5,54) = 3.67$, $p = 0.006$. SMN had a longer mean lag than LIMBIC ($p = 0.004$). Additionally, LIMBIC had a shorter mean lag than ATT ($p < 0.001$) and FPN ($p = 0.002$). We observed no statistically significant

difference between networks for in-degree ($F(5,54) = 2.38$, $p < 0.051$ – session 1; $F(5,54) = 0.95$, $p < 0.454$ – session 2). See Figure 2. These findings suggest that specific networks have divergent Out-Degree and, by extension, differences in the rate of network information between networks.

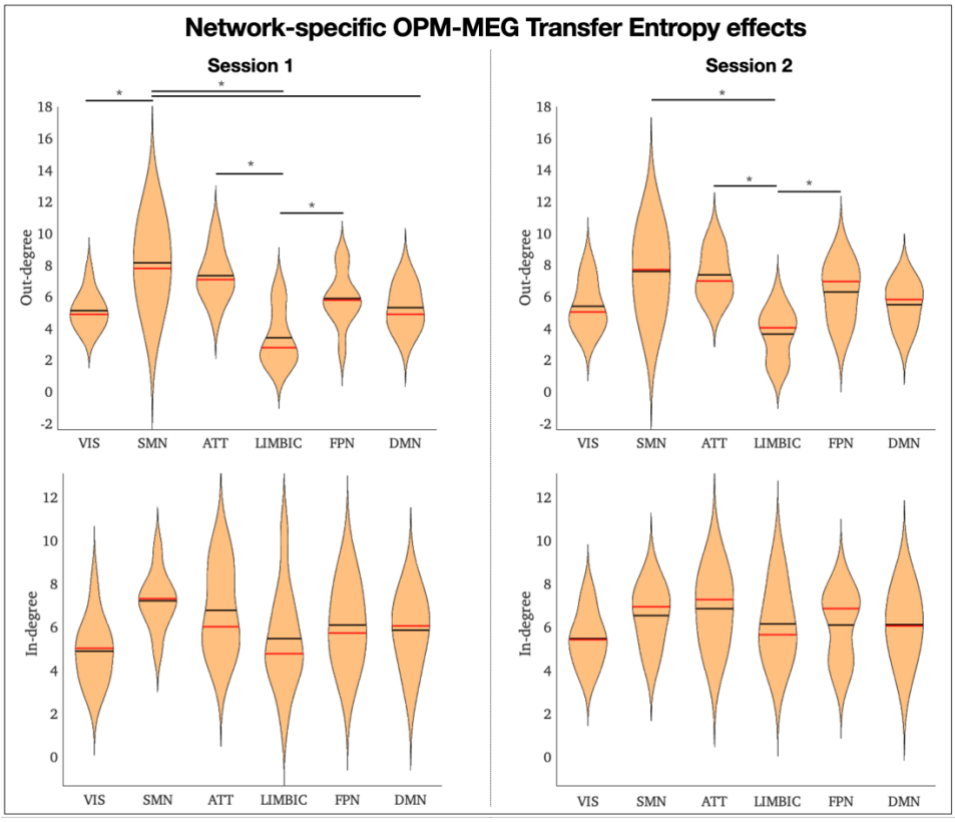

Figure 2. We calculate each subject's average Out-Degree and In-Degree within each resting-state network. Input values to ANOVA are 6 networks and 10 subjects. Lines indicate statistically significant post-hoc comparisons. Red line = mean; black line = median.

Relationship between Transfer Entropy derived In- and Out-Degree

After establishing the network-specific effects of mTE, we wanted to examine the relationship between in- and out-degree further. Firstly, we observed that Out-Degree nodes display a more heavy-tailed distribution, indicative of brain hubs, whereas in-degree nodes had a distribution closer to normal (Figure 3A). In- and Out-Degree nodes were positively correlated despite their distribution differences. Session #1: Spearman's $\rho(63) = 0.59$, $p < 0.001$. Session #2: Spearman's $\rho(63) = 0.42$, $p < 0.001$ (see Figure 3B). These findings suggest that nodes with higher In-Degree also tend to have higher Out-Degree, reflecting interconnectedness within the network. Despite the significant correlation between In- and Out-Degree, we also observed brain-specific differences between In- and Out-Degree nodes. To this end, we calculated the mean difference between In- and Out-Degree nodes. We observed that nodes in the frontal cortex have higher In-Degree and nodes across somatosensory cortices have higher Out-Degree (Figure 3C).

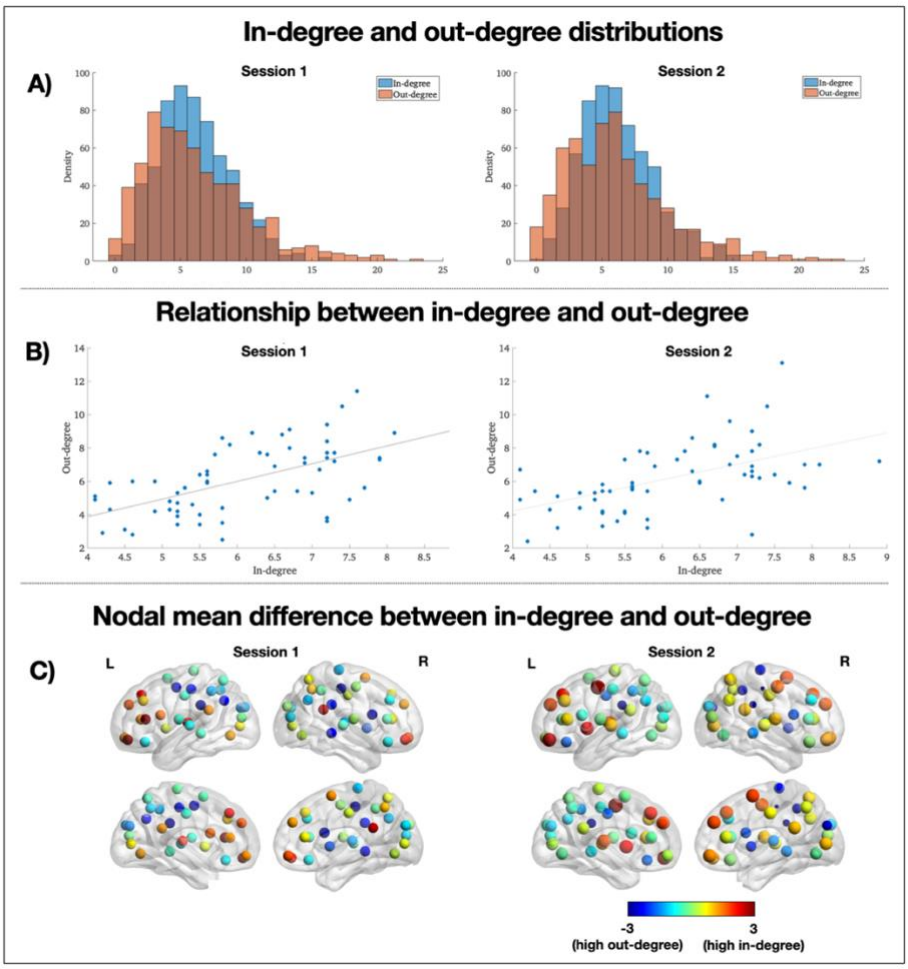

Figure 3: A) Degree distributions of all nodes from all subjects. B) Scatter-plot between In- and Out-Degree. Blue dots denote each node (here, 62 nodes), averaged over all subjects. C) Difference maps between In- and Out-Degree for each node, averaged across subjects.

mTE lags are inversely related to the physical distance between nodes.

To explore the relationship between spatial proximity and lag dynamics within the brain, we performed calculations of Euclidean distance between nodes. We examined correlations between distance and average lag values across the nodes. The results of the node-specific correlation analysis revealed significant findings in both Session #1 and Session #2. We observed a strong negative correlation, Spearman's $\rho(61) = -0.62$, $p < 0.001$ (session 1) and Spearman's $\rho(61) = -0.66$, $p < 0.001$ (session 2), indicating that shorter inter-node spatial distances were associated with higher lag values. These results are consistent with our expectations, as the sensory nodes, closely spaced together, showed higher lag structures than other regions in our previous analysis (see Figure 4). The relationship between spatial proximity and lag dynamics provides valuable insights into the organisation of information flow in the brain, particularly within the sensory networks.

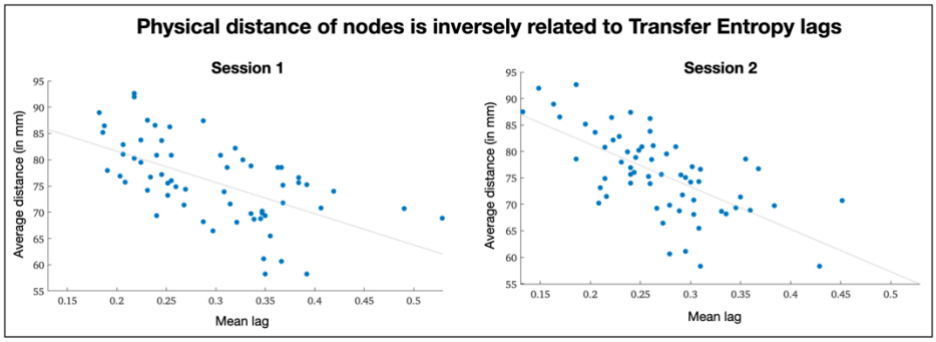

Figure 4: Scatter plots between Euclidian distance for each node (y-axis) and mean lag (an average of in and out-degree), averaged across subjects.

mTE networks have a small world topology.

Small-worldness is a fundamental topological property in biological systems and is associated with efficient local and global information processing (Watts & Strogatz, 1998). In this study, we aimed to examine the presence of small-world topology in our network by testing if its small-worldness value is above 1, which is the threshold for network small-worldness. In this analysis, we binarised mTE networks to ensure that significant mTE connections are binary with a value of 1 and non-significant connections have a value of 0.

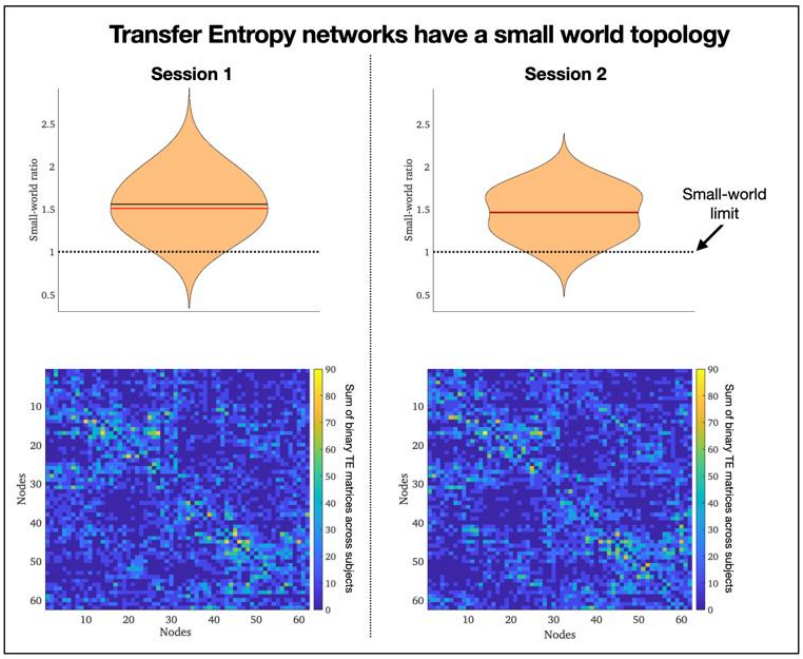

Figure 5: Top: Average whole-brain small-worldness. The stippled line shows benchmark small-worldness, as a network is deemed to have a small-world topology at values above 1. Red line = mean; black line = median. Bottom: mTE from all 10 subjects overlaid each other.

Figure 5 shows that the mTE network has a small-world topology by conducting one-sample t-tests using data from Sessions #1 and #2 (baseline value in the one-sample t-test was 1). In Session #1, the one-sample t-test yielded a significant result, $t(9) = 3.99$, $p = 0.003$, indicating that the network exhibited small-world characteristics. Similarly, in Session #2, the one-sample t-test result was also significant, $t(9) = 4.08$, $p = 0.003$, further suggesting the presence of small-worldness in the network. These findings suggest that mTE networks have a small-world topology with high local connectedness and efficient information propagation.

mTE shows converging information with Phase Lag index and Pearson Correlation Coefficient

Lastly, we wanted to measure the similarity between mTE and Phase Lag Index (a non-directed measure of lagged functional connectivity – Stam et al., 2007) and the Pearson correlation coefficient. We chose the Phase Lag Index as we hypothesised this metric is similar, albeit undirected, to mTE, and we chose the correlation coefficient as it is mathematically dissimilar to mTE in capturing zero-lag correlations. Given that our mTE matrices denote statistically significant lag indices (and not connectivity strength per se), we analysed the phase lag index between brain connections with significant and non-significant mTE. For both sessions, we observed that the Phase Lag Index was higher for connections with significant mTE compared to connections with non-significant mTE (Session 1: Paired t-test, $t(9) = 20.1$, $p < 0.001$. Session 2: Paired t-test, $t(9) = 16.7$, $p < 0.001$ – see Figure 6).

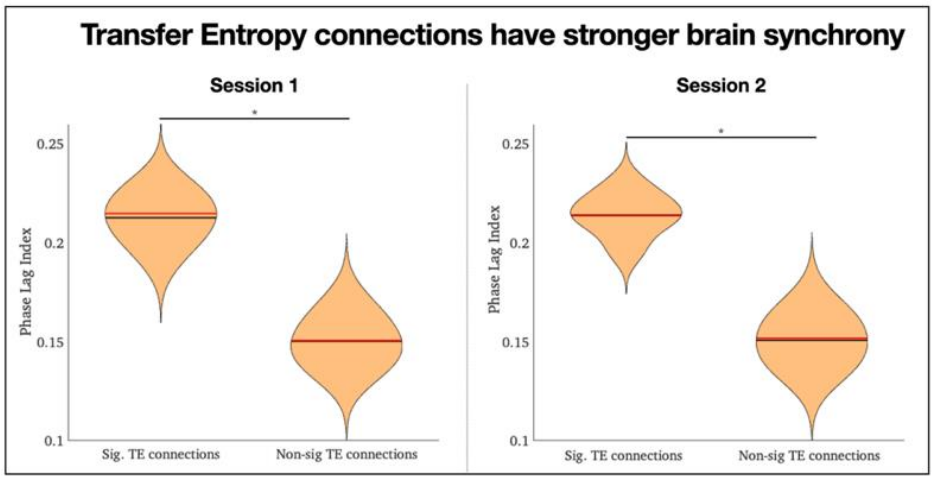

Figure 6: Phase lag index differences between significant and non-significant mTE connections. Between. The line indicates a statistically significant paired t-test. Red line = mean; black line = median.

We also observed similar results for the Pearson correlation coefficient with greater correlation for connections with significant mTE, compared to connections with non-significant mTE (Session 1: Paired t-test, $t(9) = 10.9$, $p < 0.001$. Session 2: Paired t-test, $t(9) = 8.6$, $p < 0.001$ – see Figure 6). These findings suggest that connections exhibiting significant lag indices in the mTE matrices also display distinctive functional connectivity patterns in terms of phase relationships captured by the PLI and correlations captured by Pearson's correlation coefficient.

Inter-hemispheric analysis of mTE

We also investigated whether there is any inter-hemispheric asymmetry of mTE matrices, but we found no differences between 31 right hemisphere nodes and homologous left hemisphere nodes ($t(9) = -0.27$, $p = 0.791$ – session 1; $t(9) = -1.22$, $p = 0.254$ – session 2).

mTE similarity between the two scanning sessions

Although the sample size is limited to conducting intra-class coefficient analysis for test-retest reliability, we calculated the correlation between the two OPM-MEG sessions between all mTE connections (see Figure 7). We observed consistently high correlations for connections (Spearman's $\rho > 0.8$), a finding that agrees with a previous analysis by Rier et al. (2023).

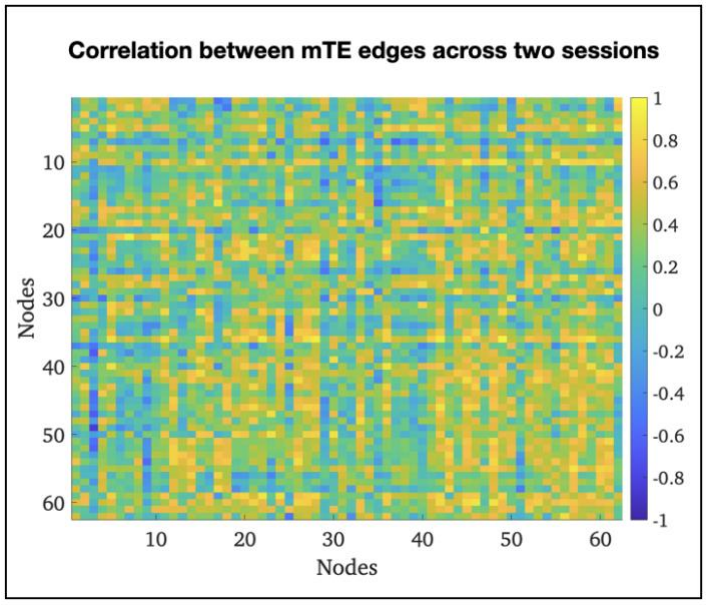

Figure 7: Correlation between the two sessions (N=10), for all mTE edges.

Discussion

OPM-MEG is an exciting development in human neuroscience as it provides a wearable design and a high temporal resolution while being less susceptible to volume conduction than EEG (Brookes et al., 2022). This feasibility study is preliminary validation for directed connectivity studies with OPM-MEG.

We observed a positive correlation between In- and Out-Degree nodes, indicating that nodes with many incoming connections also have many outgoing connections (Figure 3B). These highly connected nodes likely serve as brain hubs interconnecting diverging networks, as is common in networks with heavy-tailed degree distributions (Figure 3A – see Heuvel & Sporns, 2011). Brain hubs are found within small-world networks, a characteristic that aligns with our research findings, indicating that mTE networks exhibit a small-world topology (Figure 5). This suggests that mTE networks are biologically valid and characterized by high nodal clustering and low path length. Connections with significant mTE also displayed stronger functional connectivity, as shown by non-directional measures, Phase Lag Index (Figure 6) and Pearson's correlation coefficient. This finding suggests that mTE will likely share similar properties with non-directed connectivity measures. Most brain connectivity measures used in human neuroscience are undirected, meaning they do not provide information about the directionality of the flow (Rubinov & Sporns, 2010). However, TE provides a valuable tool to investigate directed connectivity, enabling us to gain insights into the specific pathways of information transfer between brain regions. This aspect of TE enhances our understanding of the underlying neural dynamics and mechanisms of communication within the brain. Another strength of mTE is its ability to overcome the issue of zero-lag connectivity, which is often associated with spurious activity and source leakage between local sources in MEG data, leading to misleading connectivity estimations (Brookes et al., 2012). Our findings were repeatable across two scanning sessions for most brain connections (see Figure 7), consistent with previous work, with a strong mTE correlation between OPM-MEG scans (Rier et al., 2023). We believe more extensive studies are needed to confirm the reliability of connectivity measures in OPM-MEG.

Our findings suggest that specific networks, particularly the Sensorimotor network, have higher out-degrees than other networks (Figure 2). Considering the mTE-based lags as a potential proxy for neuronal speed is tempting. Under this premise, the observed lag structure between resting state networks could offer insights into the information processing speed within neuronal circuits. Despite the spatial proximity of somatomotor areas, their circuitry spans multiple regions within cortico-striatal-thalamo-corticocircuits (Silkis, 2001), which might contribute to the negative correlation between node distance and corresponding lags (see Figure 4). However, the limited signal coverage

in deep brain regions with OPM-MEG (Boto et al., 2019) presents a challenge in testing this hypothesis. Nevertheless, the future integration of OPM-MEG with diffusion MRI holds promise for investigating the potential association between white matter tract length and mTE-based lag length (Berman et al., 2016).

Several limitations need to be considered in our study. The potential concern lies in the necessary band-pass filtering and downsampling of OPM-MEG data in the context of information-theoretic approaches such as mTE or Granger Causality. There is ongoing debate regarding the impact of band-pass filtering on the results obtained from these methods (Barnett & Seth, 2011). Similarly, filtering is contraindicated in TE due to its potential to alter the temporal structure of the data (Weber et al., 2017). In our study, we needed to filter the data between 1 and 48Hz to ensure an acceptable signal-to-noise ratio, considering the narrow bandwidth limitations of the Alkali-based OPM-MEG sensors used in this study. However, it is important to acknowledge that this filtering decision represents a trade-off, and further investigations may be warranted to explore the impact of different filter settings on the TE results. We also deemed that downsampling is needed to ensure that mTE is computationally tractable for OPM-MEG data. However, we carefully considered our temporal downsampling process, ensuring that the order of downsampling was equal to the longest lag used in this study, i.e., 10, to reduce the probability of false negative connections (Weber et al., 2017).

In conclusion, OPM-MEG research is expected to experience substantial growth, and this research suggests that the use of directed connectivity measures can offer valuable insights into the mechanisms behind brain communication. These measures can enhance our understanding of information transmission and processing within the brain, contributing to advancements in neuroscientific knowledge.

Methods

Subjects

We used data from previous work (Rier et al., 2023)**,** where data was released on an open-access Zenedo repository (https://zenodo.org/records/7477061) under a Creative Commons Attribution 4.0 International licence allowing re-use of data. The study was conducted and ethically approved at the University of Nottingham. No local ethics approval was needed for this study. In brief, this study had 10 participants, 6 males and 4 females, all right-handed, who provided written informed consent to participate in the experiment. The age range of the participants was 31 ± 8 years (mean ± standard deviation across subjects).

OPM-MEG

In a magnetically shielded room, participants underwent two scanning sessions in an OPM-MEG system with 168 triaxial channels (Brookes et al., 2021). Before the OPM-MEG recording, a field-mapping and nulling procedure (Rea et al., 2021) was conducted to control the background magnetic field. Participants viewed a 600-second clip from the movie "Dog Day Afternoon" used in published papers (Haufe et al., 2018; Honey et al., 2012). Each subject underwent two scanning sessions with the same clip for both scans. The sensor helmet was not removed between scans to ensure a single co-registration of sensor geometry to brain anatomy, thereby minimising co-registration error. The time gap between the two scanning runs was approximately 1-2 minutes. This procedure ensured the accuracy and consistency of the magnetic field measurements throughout the experiment.

We pre-processed the data using MATLAB scripts (v2023a, Natick, Massachusetts) from https://github.com/LukasRier/Rier2022_OPM_connectome_test-retest/. Every participant also underwent an MRI scan, which was performed using a Phillips Ingenia 3T MRI scanner with an MPRAGE sequence and a 1-mm isotropic resolution. An anatomical MRI and a 3D in-line surface representation (Einscan H, SHINING 3D, Hangzhou, China) were used to co-register accurate sensor locations. A single-shell forward model was computed using a head model built using the MNI-152 template MRI with a 1 mm isotropic voxel resolution (Nolte, 2003). The source location was presented in a pseudo-Z picture reconstructed using a Linearly Constrained Minimum Variance Beamforming beamformer. We calculated the average Beamformed signal in 62 cortical nodes (based on the AAL parcellation mask – Tzourio-Mazoyer et al., 2002). We applied a notch filter at 50Hz before additionally band-pass filtering the OPM-MEG time series between 1 and 48 data using a 4th-order Butterworth Filter. More information on the OPM-MEG system used in this study can be found in Rier et al. (2023).

Multivariate Transfer Entropy (mTE)

We used mTE in this study as it has higher specificity with increasing time points relative to a bivariate version of TE (Novelli & Lizier, 2021). Instead of considering isolated pairs of nodes, mTE aims to model the system by identifying a minimal set of sources that collectively contribute to the target's next state (Novelli et al., 2019). This approach is based on information theory and proposes that the next step of a target source is the composite of past information (H_t), with information transferred ($T_{x \to y(t)}$) from other sources and intrinsic uncertainty (C) (see Schreiber, 2000):

$$y_{t+1} = H_t + T_{x \to y(t)} + C$$

For mTE, the goal for each target is to identify the smallest number of sources $X_{<t}$ that maximises the collective entropy of Υ, where I is conditional mutual information:

$$mTE_{X \to \Upsilon(t)} \coloneqq I(X_{<t}; \Upsilon_t | \Upsilon_{<t})$$

The algorithm uses a non-uniform embedding of a target's previous state, $\Upsilon_{<t}$, and a greedy approach is used to iteratively select candidate variables from a set of lagged variables from the past of each target and source. The greedy algorithm has several steps: (1) Evaluating the transfer entropy of all possible source nodes to a target note (2) Select for inclusion a source that accounts for the largest amount of incremental information about the next time step of the target node (3) repeat steps 1 and 2 until no significant additions can be made or all possible sources are included. Computational complexity is further addressed using set lags to restrict the field of possible time steps in the past likely contributing sources. The minimum lag in this study is 1 time point, and the maximum lag is 10 time points. Candidate variables are added to $X_{<t}$, excluding Υ. A minimum statistic test was used to remove redundant sources in selecting past variables as part of the greedy algorithm. Final source selection was conducted with an Omnibus test that evaluates each calculated TE source against a null distribution with 200 randomisations in the embedding space under the assumption that no information is being transferred between signals. mTE was computed using the IDTxl toolbox to measure the directed connectivity. We used a Gaussian estimator for mTE. Although mTE is model-free, previous research has shown that Gaussian TE is equivalent to Granger Causality (Barnett et al., 2009), a well-established measure to assess directed relationships among time series variables (Granger, 1969).

We observed that over 80% of all significant Transfer Entropy connections had short lags within 1 or 2-time points with a heavy-tailed distribution towards a lag of 10-time points. Since mTE employs an in-build statistical procedure pruning connections in the network (Novelli et al., 2019)**,** we observed that there were slight differences in network density between subjects (network density session 1 = 9.5% ± 2.2; and network density session 2 = 9.8% ± 2.3):

Phase Lag Index and Pearson Correlation Coefficient

To compare mTE to other connectivity measures, we choose the Phase Lag Index and Pearson Correlation Coefficient. PLI is a non-directed measure quantifying the lagged synchronicity between sources (Stam et al., 2007). It captures the phase differences between source pairs after a Hilbert transform of the time series (Bedrosian, 1963; Venouziou & Zhang, 2008). Phase Lag Index, or PLI is defined as,

$$PLI = |sgsn(\sin(\Delta\phi))|,$$

where the signum function ($sgsn$) is used to ensure that values close to 0 mod π are suppressed, as they are commonly associated with zero-lag artefacts. The imaginary component of The PLI out range between 0 (no synchronicity) and 1 (full synchronicity) between time series, t_k.

Pearson's correlation coefficient captures zero-lag relationships between variables and is, therefore, conceptually different than mTE and PLI. Pearson's correlation coefficient, *r*, is defined as:

$$r = \frac{\sum(x_i - \bar{x})(y_i - \bar{y})}{\sqrt{\sum(x_i - \bar{x})^2 \sum(y_i - \bar{y})^2}},$$

Where x_i and y_i are OPM-MEG time-points from two sources, and $\bar{x}$ and $\bar{y}$ are the average of the entire time-series.

Graph theoretic metrics

To take full advantage of the asymmetric nature of mTE networks, we calculated graph measures with directed information by computing the In-Degree (incoming information to nodes) and Out-Degree (outgoing information to nodes). See Rubinov & Sporns (2010), for more information. In-Degree is calculated as $k_i^{in} = \sum_{j=1}^{G} a_{ji}$, and Out-Degree is calculated as $k_i^{out} = \sum_{j=1}^{G} a_{ij}$,. With G being the size of the network (here 62 nodes or sources), as the sum of lags are measured in the network (a_{ij} and a_{ji}, respectively). Note that a_{ij} and a_{ji} are not equal and result in directional connectivity information. To determine whether mTE networks have a small-world topology, we binarised networks and used the network weights for analysis, i.e., an undirected version of the

matrices. Small-worldness is estimated as the ratio between the normalised clustering coefficient and normalised path length (Watts & Strogatz, 1998). The clustering coefficient estimates the local connectedness in a network and is formulated as follows:

$$CC_i = \frac{1}{n}\sum_{i \in N} \frac{2t_i}{k(k_i - 1)},$$

where t_i denotes the number of nodes forming connected triangles surrounding node *i*, and k is the total degree of node *i*. The shortest path length (PL) measures the network's overall information transfer efficiency. It is defined as:

$$PL_i = \sum_{j=1}^{N} \frac{p_{ij}}{N-1,},$$

p is the number of nodes or steps in the network that separate two connected nodes (p_{ij}). CC and PL were normalised by dividing the original values with an estimate from randomising the original matrices 500 times. Small-worldness was averaged across all nodes in our analysis and is defined as:

$$SW = \frac{CC/CC_{rand}}{PL/PL_{rand}}.$$

Statistical analysis

To estimate lag differences between resting-state networks, we employed a 1x6 ANOVA, and multiple comparisons testing was assessed with Tukey's test. A one-sample t-test was used to determine whether mTE networks have a small-world topology, comparing empirical small-world values to 1 (as values above 1 indicate that a network has a small-world topology). A paired-sample t-test was used to quantify the relationship between significant/non-significant mTE networks and the Phase Lag Index and Pearson's correlation coefficient, as the same subjects are in these conditions. Spearman's rho correlations were used to quantify the relationships between In- and Out-Degree, Physical length between nodes, and average lag across nodes.

References

Barnett, L., Barrett, A. B., & Seth, A. K. (2009). Granger Causality and Transfer Entropy Are Equivalent for Gaussian Variables. *Physical Review Letters*, *103*(23), 238701. https://doi.org/10.1103/PhysRevLett.103.238701

Barnett, L., & Seth, A. K. (2011). Behaviour of Granger causality under filtering: Theoretical invariance and practical application. *Journal of Neuroscience Methods*, *201*(2), 404–419. https://doi.org/10.1016/j.jneumeth.2011.08.010

Bedrosian, E. (1963). A product theorem for Hilbert transforms. *Proceedings of the IEEE*, *51*(5), 868–869. https://doi.org/10.1109/PROC.1963.2308

Betzel, R. F., Griffa, A., Avena-Koenigsberger, A., Goñi, J., Thiran, J.-P., Hagmann, P., & Sporns, O. (2013). Multi-scale community organization of the human structural connectome and its relationship with resting-state functional connectivity. *Network Science*, *1*(3), 353–373. https://doi.org/10.1017/nws.2013.19

Boto, E., Hill, R. M., Rea, M., Holmes, N., Seedat, Z. A., Leggett, J., Shah, V., Osborne, J., Bowtell, R., & Brookes, M. J. (2021). Measuring functional connectivity with wearable MEG. *NeuroImage*, *230*, 117815. https://doi.org/10.1016/j.neuroimage.2021.117815

Boto, E., Holmes, N., Leggett, J., Roberts, G., Shah, V., Meyer, S. S., Muñoz, L. D., Mullinger, K. J., Tierney, T. M., Bestmann, S., Barnes, G. R., Bowtell, R., & Brookes, M. J. (2018). Moving magnetoencephalography towards real-world applications with a wearable system. *Nature*, *555*(7698), 657–661. https://doi.org/10.1038/nature26147

Boto, E., Seedat, Z. A., Holmes, N., Leggett, J., Hill, R. M., Roberts, G., Shah, V., Fromhold, T. M., Mullinger, K. J., Tierney, T. M., Barnes, G. R., Bowtell, R., & Brookes, M. J. (2019). Wearable neuroimaging: Combining and contrasting magnetoencephalography and electroencephalography. *NeuroImage*, *201*, 116099. https://doi.org/10.1016/j.neuroimage.2019.116099

Brookes, M. J., Boto, E., Rea, M., Shah, V., Osborne, J., Holmes, N., Hill, R. M., Leggett, J., Rhodes, N., & Bowtell, R. (2021). Theoretical advantages of a triaxial optically pumped magnetometer magnetoencephalography system. *NeuroImage*, *236*, 118025. https://doi.org/10.1016/j.neuroimage.2021.118025

Brookes, M. J., Leggett, J., Rea, M., Hill, R. M., Holmes, N., Boto, E., & Bowtell, R. (2022). Magnetoencephalography with optically pumped magnetometers (OPM-MEG): The next generation of functional neuroimaging. *Trends in Neurosciences*, *45*(8), 621–634. https://doi.org/10.1016/j.tins.2022.05.008

Brookes, M. J., Woolrich, M. W., & Barnes, G. R. (2012). Measuring functional connectivity in MEG: A multivariate approach insensitive to linear source leakage. *NeuroImage*, *63*(2), 910–920. https://doi.org/10.1016/j.neuroimage.2012.03.048

Bullmore, E., & Sporns, O. (2009). Complex brain networks: Graph theoretical analysis of structural and functional systems. *Nature Reviews. Neuroscience*, *10*(3), 186–198. https://doi.org/10.1038/nrn2575

Feys, O., Corvilain, P., Aeby, A., Sculier, C., Holmes, N., Brookes, M., Goldman, S., Wens, V., & De Tiège, X. (2022). On-Scalp Optically Pumped Magnetometers versus Cryogenic Magnetoencephalography for Diagnostic Evaluation of Epilepsy in School-aged Children. *Radiology*, *304*(2), 429–434. https://doi.org/10.1148/radiol.212453

Fourcault, W., Romain, R., Gal, G. L., Bertrand, F., Josselin, V., Prado, M. L., Labyt, E., & Palacios-Laloy, A. (2021). Helium-4 magnetometers for room-temperature biomedical imaging: Toward collective operation and photon-noise limited sensitivity. *Optics Express*, *29*(10), 14467–14475. https://doi.org/10.1364/OE.420031

Granger, C. W. J. (1969). Investigating Causal Relations by Econometric Models and Cross-spectral Methods. *Econometrica*, *37*(3), 424–438. https://doi.org/10.2307/1912791

Haufe, S., DeGuzman, P., Henin, S., Arcaro, M., Honey, C. J., Hasson, U., & Parra, L. C. (2018). Elucidating relations between fMRI, ECoG, and EEG through a common natural stimulus. *NeuroImage*, *179*, 79–91. https://doi.org/10.1016/j.neuroimage.2018.06.016

Heuvel, M. P. van den, & Sporns, O. (2011). Rich-Club Organization of the Human Connectome. *Journal of Neuroscience*, *31*(44), 15775–15786. https://doi.org/10.1523/JNEUROSCI.3539-11.2011

Hill, R. M., Boto, E., Rea, M., Holmes, N., Leggett, J., Coles, L. A., Papastavrou, M., Everton, S. K., Hunt, B. A. E., Sims, D., Osborne, J., Shah, V., Bowtell, R., & Brookes, M. J. (2020). Multi-channel whole-head OPM-MEG: Helmet design and a comparison with a conventional system. *NeuroImage*, *219*, 116995. https://doi.org/10.1016/j.neuroimage.2020.116995

Hill, R. M., Devasagayam, J., Holmes, N., Boto, E., Shah, V., Osborne, J., Safar, K., Worcester, F., Mariani, C., Dawson, E., Woolger, D., Bowtell, R., Taylor, M. J., & Brookes, M. J. (2022). Using OPM-MEG in contrasting magnetic environments. *NeuroImage*, *253*, 119084. https://doi.org/10.1016/j.neuroimage.2022.119084

Holmes, N., Rea, M., Chalmers, J., Leggett, J., Edwards, L. J., Nell, P., Pink, S., Patel, P., Wood, J., Murby, N., Woolger, D., Dawson, E., Mariani, C., Tierney, T. M., Mellor, S., O'Neill, G. C., Boto, E., Hill, R. M., Shah, V., … Bowtell, R. (2022). A lightweight magnetically shielded room with active shielding. *Scientific Reports*, *12*(1), Article 1. https://doi.org/10.1038/s41598-022-17346-1

Honey, C. J., Thesen, T., Donner, T. H., Silbert, L. J., Carlson, C. E., Devinsky, O., Doyle, W. K., Rubin, N., Heeger, D. J., & Hasson, U. (2012). Slow Cortical Dynamics and the Accumulation of Information over Long Timescales. *Neuron*, *76*(2), 423–434. https://doi.org/10.1016/j.neuron.2012.08.011

Iivanainen, J., Zetter, R., Grön, M., Hakkarainen, K., & Parkkonen, L. (2019). On-scalp MEG system utilizing an actively shielded array of optically-pumped magnetometers. *NeuroImage*, *194*, 244–258. https://doi.org/10.1016/j.neuroimage.2019.03.022

Jas, M., Jones, S. R., & Hämäläinen, M. S. (2021). Whole-head OPM-MEG enables noninvasive assessment of functional connectivity. *Trends in Neurosciences*, *44*(7), 510–512. https://doi.org/10.1016/j.tins.2021.04.006

Mellor, S. J., Tierney, T., O'Neill, G., Alexander, N., Seymour, R., Holmes, N., Lopez, J. D., Hill, R., Boto, E., Rea, M., Roberts, G., Leggett, J., Bowtell, R., Brookes, M. J., Maguire, E., Walker, M., & Barnes, G. (2021). Magnetic Field Mapping and Correction for Moving OP-MEG. *IEEE Transactions on Biomedical Engineering*, 1–1. https://doi.org/10.1109/TBME.2021.3100770

Mellor, S., Vivekananda, U., O'Neill, G. C., Tierney, T. M., Doig, D., Seymour, R. A., Alexander, N., Walker, M. C., & Barnes, G. R. (2021). *First experiences of whole-head OP-MEG recordings from a patient with Epilepsy* (p. 2021.09.28.21264047). https://doi.org/10.1101/2021.09.28.21264047

Nolte, G. (2003). The magnetic lead field theorem in the quasi-static approximation and its use for magnetoencephalography forward calculation in realistic volume conductors. *Physics in Medicine and Biology*, *48*(22), 3637–3652. https://doi.org/10.1088/0031-9155/48/22/002

Novelli, L., & Lizier, J. T. (2021). Inferring network properties from time series using transfer entropy and mutual information: Validation of multivariate versus bivariate approaches. *Network Neuroscience (Cambridge, Mass.)*, *5*(2), 373–404. https://doi.org/10.1162/netn_a_00178

Novelli, L., Wollstadt, P., Mediano, P., Wibral, M., & Lizier, J. T. (2019). Large-scale directed network inference with multivariate transfer entropy and hierarchical statistical testing. *Network Neuroscience (Cambridge, Mass.)*, *3*(3), 827–847. https://doi.org/10.1162/netn_a_00092

Pedersen, M., Abbott, D. F., & Jackson, G. D. (2022). Wearable OPM-MEG: A changing landscape for epilepsy. *Epilepsia*, *63*(11), 2745–2753. https://doi.org/10.1111/epi.17368

Rea, M., Holmes, N., Hill, R. M., Boto, E., Leggett, J., Edwards, L. J., Woolger, D., Dawson, E., Shah, V., Osborne, J., Bowtell, R., & Brookes, M. J. (2021). Precision magnetic field modelling and control for wearable magnetoencephalography. *NeuroImage*, *241*, 118401. https://doi.org/10.1016/j.neuroimage.2021.118401

Rier, L., Michelmann, S., Ritz, H., Shah, V., Hill, R. M., Osborne, J., Doyle, C., Holmes, N., Bowtell, R., Brookes, M. J., Norman, K. A., Hasson, U., Cohen, J. D., & Boto, E. (2023). Test-retest reliability of the human connectome: An OPM-MEG study. *Imaging Neuroscience*, *1*, 1–20. https://doi.org/10.1162/imag_a_00020

Roberts, G., Holmes, N., Alexander, N., Boto, E., Leggett, J., Hill, R. M., Shah, V., Rea, M., Vaughan, R., Maguire, E. A., Kessler, K., Beebe, S., Fromhold, M., Barnes, G. R., Bowtell, R., & Brookes, M. J. (2019). Towards OPM-MEG in a virtual reality environment. *NeuroImage*, *199*, 408–417. https://doi.org/10.1016/j.neuroimage.2019.06.010

Rubinov, M., & Sporns, O. (2010). Complex network measures of brain connectivity: Uses and interpretations. *NeuroImage*, *52*(3), 1059–1069. https://doi.org/10.1016/j.neuroimage.2009.10.003

Schreiber, T. (2000). Measuring Information Transfer. *Physical Review Letters*, *85*(2), 461–464. https://doi.org/10.1103/PhysRevLett.85.461

Seymour, R. A., Alexander, N., Mellor, S., O'Neill, G. C., Tierney, T. M., Barnes, G. R., & Maguire, E. A. (2022). Interference suppression techniques for OPM-based MEG: Opportunities and challenges. *NeuroImage*, *247*, 118834. https://doi.org/10.1016/j.neuroimage.2021.118834

Sporns, O. (2013). Network attributes for segregation and integration in the human brain. *Current Opinion in Neurobiology*, *23*(2), 162–171. https://doi.org/10.1016/j.conb.2012.11.015

Stam, C. J., Nolte, G., & Daffertshofer, A. (2007). Phase lag index: Assessment of functional connectivity from multi channel EEG and MEG with diminished bias from common sources. *Human Brain Mapping*, *28*(11), 1178–1193. https://doi.org/10.1002/hbm.20346

Tierney, T. M., Holmes, N., Mellor, S., López, J. D., Roberts, G., Hill, R. M., Boto, E., Leggett, J., Shah, V., Brookes, M. J., Bowtell, R., & Barnes, G. R. (2019). Optically pumped magnetometers: From quantum origins to multi-channel magnetoencephalography. *NeuroImage*, *199*, 598–608. https://doi.org/10.1016/j.neuroimage.2019.05.063

Tzourio-Mazoyer, N., Landeau, B., Papathanassiou, D., Crivello, F., Etard, O., Delcroix, N., Mazoyer, B., & Joliot, M. (2002). Automated anatomical labeling of activations in SPM using a macroscopic anatomical parcellation of the MNI MRI single-subject brain. *NeuroImage*, *15*(1), 273–289. https://doi.org/10.1006/nimg.2001.0978

van den Heuvel, M. P., Stam, C. J., Boersma, M., & Hulshoff Pol, H. E. (2008). Small-world and scale-free organization of voxel-based resting-state functional connectivity in the human brain. *NeuroImage*, *43*(3), 528–539. https://doi.org/10.1016/j.neuroimage.2008.08.010

Venouziou, M., & Zhang, H. (2008). Characterizing the Hilbert transform by the Bedrosian theorem. *Journal of Mathematical Analysis and Applications*, *338*(2), 1477–1481. https://doi.org/10.1016/j.jmaa.2007.05.067

Vivekananda, U., Mellor, S., Tierney, T. M., Holmes, N., Boto, E., Leggett, J., Roberts, G., Hill, R. M., Litvak, V., Brookes, M. J., Bowtell, R., Barnes, G. R., & Walker, M. C. (2020). Optically pumped magnetoencephalography in epilepsy. *Annals of Clinical and Translational Neurology*, *7*(3), 397–401. https://doi.org/10.1002/acn3.50995

Watts, D. J., & Strogatz, S. H. (1998). Collective dynamics of ‘small-world’ networks. *Nature*, *393*(6684), 440–442. https://doi.org/10.1038/30918

Weber, I., Florin, E., von Papen, M., & Timmermann, L. (2017). The influence of filtering and downsampling on the estimation of transfer entropy. *PloS One*, *12*(11), e0188210. https://doi.org/10.1371/journal.pone.0188210

Wollstadt, P., Lizier, J. T., Vicente, R., Finn, C., Martínez-Zarzuela, M., Mediano, P., Novelli, L., & Wibral, M. (2019). IDTxl: The Information Dynamics Toolkit xl: a Python package for the efficient analysis of multivariate information dynamics in networks. *Journal of Open Source Software*, *4*(34), 1081. https://doi.org/10.21105/joss.01081

Yeo, B. T. T., Krienen, F. M., Sepulcre, J., Sabuncu, M. R., Lashkari, D., Hollinshead, M., Roffman, J. L., Smoller, J. W., Zöllei, L., Polimeni, J. R., Fischl, B., Liu, H., & Buckner, R. L. (2011). The organization of the human cerebral cortex estimated by intrinsic functional connectivity. *Journal of Neurophysiology*, *106*(3), 1125–1165. https://doi.org/10.1152/jn.00338.2011

Young, J. C., Paolini, A. G., Pedersen, M., & Jackson, G. D. (2019). Genetic absence epilepsy: Effective connectivity from piriform cortex to mediodorsal thalamus. *Epilepsy & Behavior*, *97*, 219–228.